

JUN 11 1976
MAR 16 1967

AEDC-TR-76-22

cy. 8



A WIND TUNNEL CAPTIVE AIRCRAFT TESTING TECHNIQUE

PROPULSION WIND TUNNEL FACILITY
ARNOLD ENGINEERING DEVELOPMENT CENTER
AIR FORCE SYSTEMS COMMAND
ARNOLD AIR FORCE STATION, TENNESSEE 37389

April 1976

Final Report for Period 1 July 1974 — 30 June 1975

Approved for public release; distribution unlimited.

Property of U. S. Air Force
AEDC LIBRARY
F40600-75-C-0001

Prepared for

DIRECTORATE OF TECHNOLOGY (DY)
ARNOLD ENGINEERING DEVELOPMENT CENTER
ARNOLD AIR FORCE STATION, TENNESSEE 37389

NOTICES

When U. S. Government drawings specifications, or other data are used for any purpose other than a definitely related Government procurement operation, the Government thereby incurs no responsibility nor any obligation whatsoever, and the fact that the Government may have formulated, furnished, or in any way supplied the said drawings, specifications, or other data, is not to be regarded by implication or otherwise, or in any manner licensing the holder or any other person or corporation, or conveying any rights or permission to manufacture, use, or sell any patented invention that may in any way be related thereto.

Qualified users may obtain copies of this report from the Defense Documentation Center.

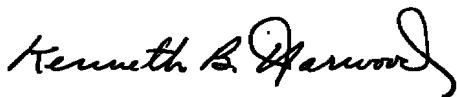
References to named commercial products in this report are not to be considered in any sense as an endorsement of the product by the United States Air Force or the Government.

This report has been reviewed by the Information Office (OI) and is releasable to the National Technical Information Service (NTIS). At NTIS, it will be available to the general public, including foreign nations.


APPROVAL STATEMENT

This technical report has been reviewed and is approved for publication.

FOR THE COMMANDER



KENNETH B. HARWOOD
Major, CF
Research & Development
Division
Directorate of Technology



ROBERT O. DIETZ
Director of Technology

UNCLASSIFIED

REPORT DOCUMENTATION PAGE		READ INSTRUCTIONS BEFORE COMPLETING FORM
1 REPORT NUMBER AEDC-TR-76-22	2 GOVT ACCESSION NO.	3. RECIPIENT'S CATALOG NUMBER
4 TITLE (and Subtitle) A WIND TUNNEL CAPTIVE AIRCRAFT TESTING TECHNIQUE		5 TYPE OF REPORT & PERIOD COVERED Final Report, 1 July 1974 - 30 June 1975
7 AUTHOR(s) R. W. Butler, ARO, Inc.		6 PERFORMING ORG. REPORT NUMBER
9 PERFORMING ORGANIZATION NAME AND ADDRESS Arnold Engineering Development Center (DY) Air Force Systems Command Arnold Air Force Station, TN 37389		8 CONTRACT OR GRANT NUMBER(s)
11 CONTROLLING OFFICE NAME AND ADDRESS Arnold Engineering Development Center (DYFS), Air Force Systems Command, Arnold Air Force Station, TN 37389		10 PROGRAM ELEMENT PROJECT, TASK AREA & WORK UNIT NUMBERS Program Element 65807F
14 MONITORING AGENCY NAME & ADDRESS (if different from Controlling Office)		12. REPORT DATE April 1976
		13. NUMBER OF PAGES 34
		15. SECURITY CLASS. (of this report) UNCLASSIFIED
		15a DECLASSIFICATION/DOWNGRADING SCHEDULE N/A
16 DISTRIBUTION STATEMENT (of this Report) Approved for public release; distribution unlimited.		
17 DISTRIBUTION STATEMENT (of the abstract entered in Block 20, if different from Report)		
18 SUPPLEMENTARY NOTES Available in DDC.		
19 KEY WORDS (Continue on reverse side if necessary and identify by block number) F-15 aircraft wind tunnel captive tests remotely piloted vehicle (RPV) flight testing external stores motion simulation flight characteristics		
20 ABSTRACT (Continue on reverse side if necessary and identify by block number) A captive aircraft testing technique has been developed for use in the 16-ft wind tunnels at the Arnold Engineering Development Center (AEDC). With the captive system, an aircraft motion study may be conducted in the wind tunnel with the tunnel acting as an analog forcing function. The large static aerodynamic data matrix normally required for a motion study has been alleviated. The system validity is established by a comparison of F-15		

UNCLASSIFIED

UNCLASSIFIED

20. ABSTRACT (Continued)

aircraft motion generated in the wind tunnel with flight motion of a NASA 3/8-scale F-15 Remotely Piloted Vehicle (RPV). Good agreement between the longitudinal and lateral/directional motions of the model was achieved in the absence of RPV unsteady aerodynamics (wing buffet). The captive technique ability to efficiently define changes in aircraft flight characteristics resulting from different external store configurations is demonstrated.

PREFACE

The work reported herein was conducted by the Arnold Engineering Development Center (AEDC), Air Force Systems Command (AFSC), under Program Element 65807F. The results of the research were obtained by ARO, Inc. (a subsidiary of Sverdrup & Parcel and Associates, Inc.), contract operator of AEDC, AFSC, Arnold Air Force Station, Tennessee. The research associated with the development of the technique was conducted under ARO Project Number P32A-33A. Testing was conducted January 20-21, 1975, under ARO Project Number P41T-78A. The author of this report was R. W. Butler, ARO, Inc. The manuscript (ARO Control No. ARO-PWT-TR-75-80) was submitted for publication on June 17, 1975.

CONTENTS

	<u>Page</u>
1.0 INTRODUCTION	5
2.0 APPARATUS	
2.1 Wind Tunnel and Test Conditions	6
2.2 Model Description	6
3.0 PROCEDURE	
3.1 Data Acquisiton	10
3.2 Precision of Data	11
4.0 RESULTS AND DISCUSSION	
4.1 General	11
4.2 Flight Test-Wind Tunnel Data Correlation	13
4.3 Captive Testing Evaluation	19
5.0 CONCLUDING REMARKS	28
REFERENCES	29

ILLUSTRATIONS

Figure

1. Wind Tunnel Model	6
2. 1/20-Scale Model in the Tunnel 16T Test Section	7
3. Horizontal Stabilizer Planform	7
4. MK-82 Bomb Assembly	8
5. MK-82 Bomb Configuration	9
6. 600-gal Tank Assembly	9
7. Captive Installation and a Block Diagram of the Computer Control Loop	10
8. Dynamic Stability Derivatives Representative of the NASA RPV Model	13
9. Flight/Wind Tunnel Correlation of Aircraft Longitudinal Motion	14
10. Flight/Wind Tunnel Correlation of Aircraft Lateral Motion	14
11. Model Trim Angle of Attack	16
12. Flight/Wind Tunnel Correlation of the Aircraft Wind-Up Turn Maneuver	17
13. Simulated RPV Lateral/Directional Motion	18

<u>Figure</u>	<u>Page</u>
14. Lateral/Directional Motion of the F-15 Model with MK-82 Store Configuration	20
15. Damping and Frequency of the F-15 Model Motion with MK-82 Stores	23
16. Lateral/Directional Motion of the F-15 Model with 600-gal Tanks	25
17. Damping and Frequency of the F-15 Model Motion with 600-gal Tanks	28

TABLE

1. Characteristics of the F-15 Aircraft Simulated in Captive Testing	12
---	----

APPENDIX

A. EQUATIONS OF MOTION	31
NOMENCLATURE	32

1.0 INTRODUCTION

When an aircraft experiences an external configuration change (addition of stores or airframe modification), the aerodynamic data matrix used to describe the aircraft in analytical motion simulation is often invalidated. In the past, the aerodynamicist has modified the original data matrix to account for configuration changes either empirically or by acquiring new aerodynamic data from additional wind tunnel tests (or by both means). Data changes occurring from the addition of external stores are normally defined empirically (Refs. 1 and 2) when the aircraft is operating in a cruise condition at low angles of attack. In high angle-of-attack maneuvering flight, characteristic of fighter/bomber aircraft, the added complexity in flow patterns associated with aircraft external store installations often renders the empirical correction methods unsatisfactory; therefore, the remaining alternative is additional wind tunnel testing. However, most fighter/bomber aircraft possess the capability of carrying numerous external store combinations. To generate data matrices for each configuration soon becomes unrealistic. An alternate approach for investigating an aircraft motion sensitivity to external configuration changes is through captive wind tunnel testing. Captive testing has been used successfully by the Royal Aircraft Establishment (RAE) for investigating the lateral/directional stability characteristics of aircraft (Ref. 3). A pilot test (Ref. 4) conducted in the AEDC Aerodynamic Wind Tunnel (4T) investigated captive testing as a tool for defining aircraft departure characteristics. Because of the success of these tests, the possibility of conducting aircraft motion analysis studies in the AEDC Propulsion Wind Tunnel (16T) with captive testing becomes attractive.

The captive testing technique utilizes a closed-loop system and a digital computer. The wind tunnel serves as a function generator for the aerodynamic static forces and moments. These data, along with wind tunnel operating conditions, model mass properties, dynamic stability derivatives, engine thrust, and model angular positions, are used in an online digital computer which solves the Euler equations of motion for the vehicle. Based on solutions to the equations, the model is repositioned and new aerodynamic coefficients acquired. Through such a cyclic process, an aircraft maneuver may be generated without acquiring a full matrix of aerodynamic force and moment data. It should be noted that control surface interactions (rudder and elevator) and Mach number variations can be fully simulated in captive testing.

To establish captive testing as a useful technique for conducting aircraft motion analysis studies in Tunnel 16T, tests were conducted using a 1/20-scale F-15 aircraft model for comparison with the NASA 3/8-scale F-15 Remotely Piloted Vehicle (RPV) flight motion. The motion was simulated in both longitudinal and lateral/directional planes. In addition, motion was generated representative of the lateral/directional flight characteristics of a full-scale F-15 fighter aircraft with two different external store configurations.

2.0 APPARATUS

2.1 WIND TUNNEL AND TEST CONDITIONS

The Propulsion Wind Tunnel (16T) is a variable-density, continuous flow wind tunnel capable of being operated at Mach numbers from 0.20 to 1.60. The test section is 16 by 16 ft in cross section and 40 ft long. The tunnel can be operated within a stagnation pressure range from 120 to 3,800 psfa, depending on Mach number.

The tests were conducted at Mach numbers from 0.15 to 0.50. Reynolds number based on the wing mean aerodynamic chord ranged from 1.3×10^6 to 2.4×10^6 . The sting support used for positioning the model is capable of pitching from -4 to 45 deg and rolling ± 180 deg. The model cross section at an angle of attack of 90 deg is one percent. Thus, because of the low blockage and low Mach numbers of the test, no wind tunnel blockage corrections are required. Flow angularity corrections were applied as a function of Mach number and model vertical position from the tunnel centerline.

2.2 MODEL DESCRIPTION

The wind tunnel data presented herein were obtained with a $1/20$ -scale model of the F-15 fighter aircraft shown in Fig. 1. The model installed in the test section is shown in Fig. 2. The two horizontal stabilizer configurations shown in Fig. 3 were used during testing. The stabilizers were moveable and remotely controlled with either differential or simultaneous deflections. Stabilizer deflections were from 5 deg trailing edge down to -25 deg up.

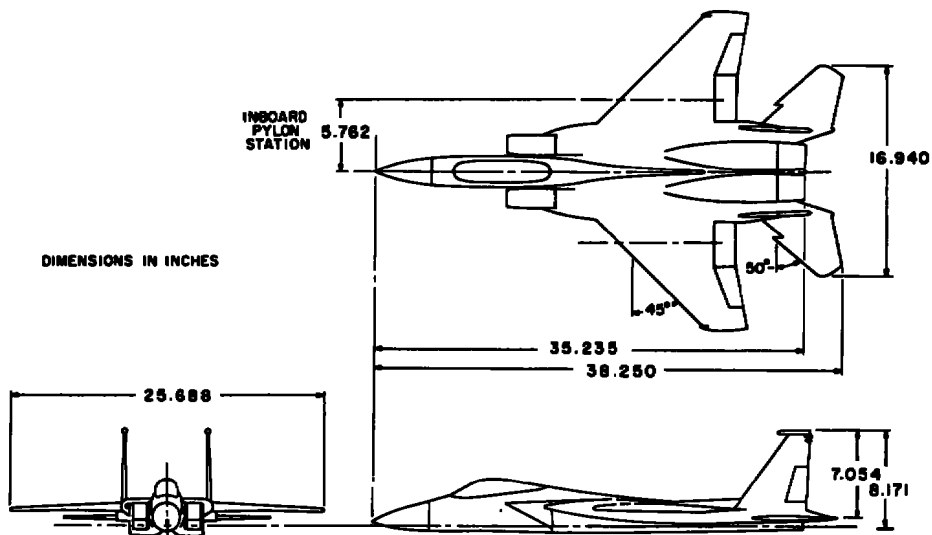


Figure 1. Wind tunnel model.

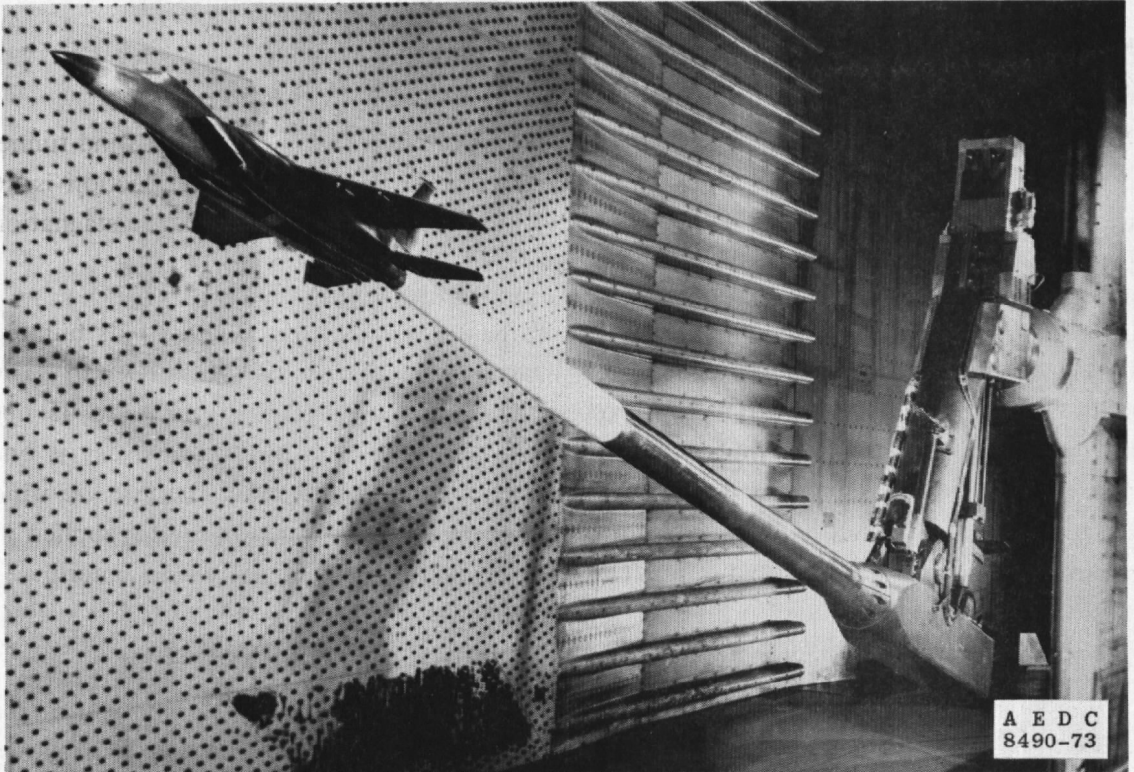
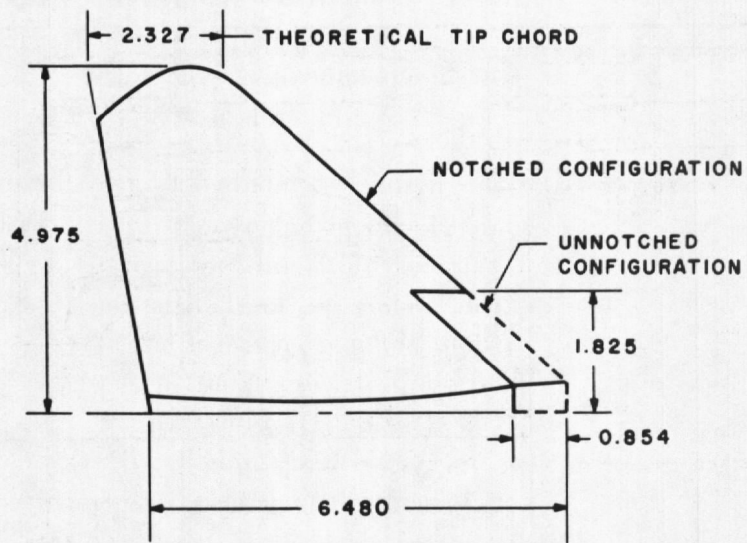


Figure 2. 1/20-scale model in the Tunnel 16T test section.



NOTE: UNNOTCHED STABILIZER HAS APPROX. 5.4% MORE AREA

Figure 3. Horizontal stabilizer planform.

Model engine inlets were in the drooped configuration, nose down, representative of the high angle-of-attack flight configuration. The inlets were plugged just inside the inlet lip, by a flat plate normal to the duct, simulating the NASA 3/8-scale F-15 inlet configuration.

The aircraft model was tested with two different external store configurations. The first configuration consisted of eighteen MK-82 bombs mounted on three multiple ejection racks (MER) located at the aircraft centerline and inboard pylon stations. The bombs, MER, and pylon assembly are shown in Fig. 4. The configuration is shown installed in the wind tunnel in Fig. 5. The second configuration consisted of two 600-gal tanks and pylons mounted on the inboard pylon stations. The model centerline station was empty. The 600-gal tank/pylon assembly is shown in Fig. 6.

A description of the NASA 3/8-scale F-15 model used to acquire the flight data presented herein is given in Ref. 5.

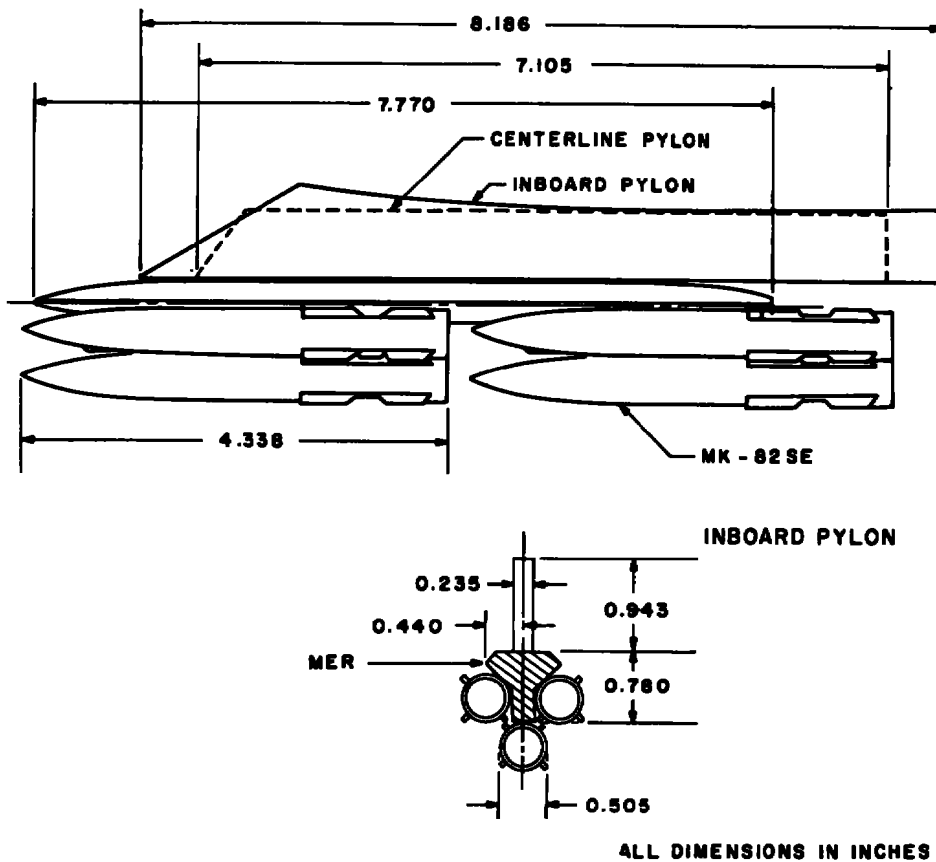
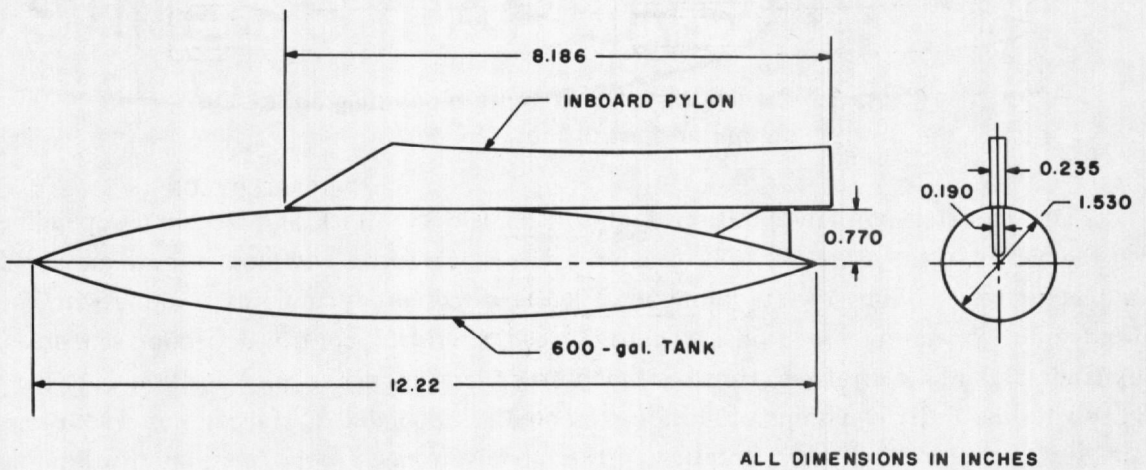


Figure 4. MK-82 bomb assembly.



Figure 5. MK-82 bomb configuration.



ALL DIMENSIONS IN INCHES

Figure 6. 600-gal tank assembly.

3.0 PROCEDURE

3.1 DATA ACQUISITION

Captive testing is accomplished through a closed-loop system consisting of the model balance, model support system, and digital computer shown in Fig. 7. The test article is installed in the wind tunnel on a six-component internal strain-gage balance. The model and balance are supported by a high pitch/roll positioning system.

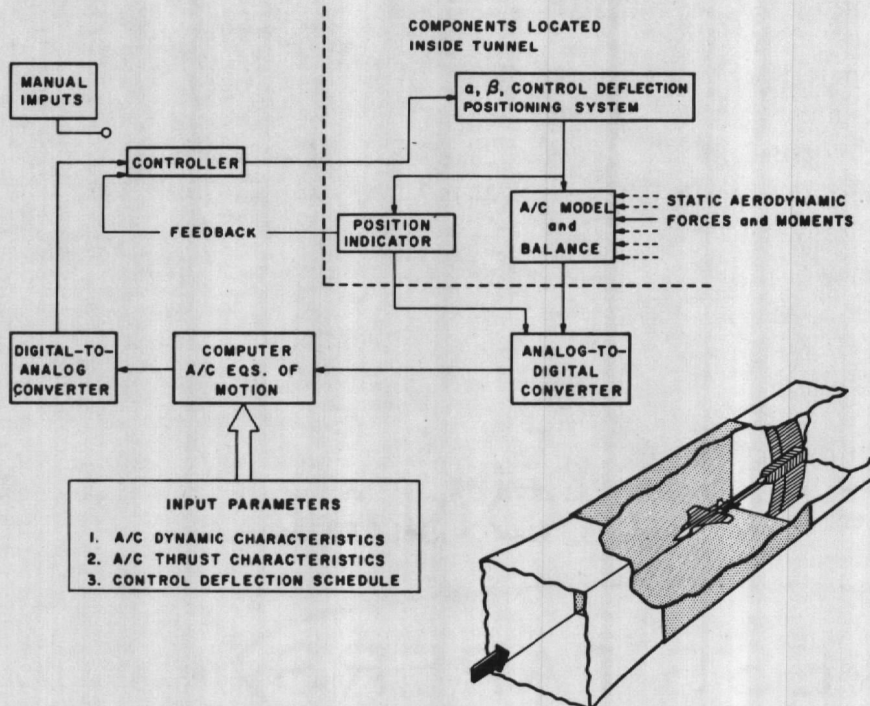


Figure 7. Captive installation and a block diagram of the computer control loop.

The model is initially positioned at some angle of attack and sideslip. Depending on the nature of the maneuver to be generated, the model forces and moments are measured and input to an online digital computer. The measured aerodynamic data, along with the wind tunnel operating conditions, model mass characteristics, control deflection schedules, dynamic stability derivatives, thrust characteristics, and model angular positions, are used in solving the Euler equations of motion presented in Appendix A. The computed solutions are used in controlling the orientation of the model through a point prediction technique (Ref. 6). The technique involves using the last two successive measured values of each static aerodynamic coefficient to predict the magnitude of the coefficient over the next

prediction interval. The prediction interval used in the subject test was 0.08 sec. The predicted coefficients are used to calculate the new model angle of attack and sideslip by integrating the equations of motion every 0.005 sec over the prediction interval. The system is then commanded to move the model to the new angular positions, and the aerodynamic loads are measured. If the new measurements agree with the predicted values, the process is continued over another prediction interval of the same magnitude. If the measured and predicted values do not agree within the specified precision, the calculations are repeated over a prediction interval one-half the previous value. This process is repeated until a complete maneuver has been obtained.

The aircraft Mach number is calculated at each prediction interval, and the wind tunnel Mach number is adjusted to within ± 0.003 of the calculated value. Thus, the aerodynamic coefficients are measured at the correct Mach number throughout the maneuver. Also, the aircraft thrust is calculated and modified with each prediction interval by mathematically modeling the simulated aircraft engine/inlet installed thrust as a function of Mach number, altitude, angle of attack, and sideslip.

The generated maneuver is a function of the control surface deflection schedule. For the subject test, the deflection schedules were input as functions of flight time, t .

3.2 PRECISION OF DATA

Maneuvers generated utilizing the captive technique are subject to error from several sources including tunnel conditions, balance measurements, extrapolation tolerances allowed in the predicted coefficients, and the angle positioning system. Mach number was measured to within ± 0.003 of the true value. Maximum error in the model positioning system was 0.1 deg for angular settings in alpha and beta. The maximum error in the position data (ψ , θ , and ϕ) caused by balance inaccuracies and coefficient prediction tolerances is estimated to be less than 1 deg.

4.0 RESULTS AND DISCUSSION

4.1 GENERAL

At the onset of the captive testing development program, a goal was established to match captive aircraft motion generated in the wind tunnel with flight motion. Because of the availability of existing wind tunnel models, availability of flight data, and minimization of Reynolds number mismatch, the NASA Edwards RPV flight program was selected for data correlation purposes. The NASA RPV is a 3/8 of full scale free-flight model of the F-15 aircraft. A description of the model is given in Ref. 5. The model is launched at high altitude (approximately 45,000 ft) from a B-52 parent aircraft. During

the model free fall, a series of maneuvers is performed encompassing the aircraft flight envelope. Time history of the model motion is recorded throughout the flight.

Although an enormous amount of RPV flight data were available prior to the wind tunnel test, only a limited portion could be utilized for data correlation because of two constraints. First, the RPV possessed a full array of remotely operated control surfaces: rudder, aileron, and differentially operated horizontal stabilizers. Because of control limitations on the 1/20-scale wind tunnel model, only flight maneuvers with no rudder and aileron movement could be compared directly with the wind tunnel data; thus a large portion of the RPV maneuvers were eliminated from consideration. The second constraint originated from the fact that the RPV could be flown via any one of four flight control systems. However, only one of these modes could be simulated with the 1/20-scale model, i.e., the computer direct mode, which provided the RPV with unaugmented proportional control. Therefore, candidate maneuvers for wind tunnel data correlation were further reduced.

The RPV mass characteristics used in generating the wind tunnel maneuvers are given in Table 1. The damping derivatives used in the motion simulation were acquired from separate wind tunnel tests and are presented in Fig. 8. Small discrepancies exist between the derivatives utilized and those extracted from RPV flight data (Ref. 5). However, the confidence level of the RPV data in areas where the discrepancies occurred (higher angle of attack) was not considered great enough to merit changing the wind tunnel predicted values. The wind tunnel time required for generating the captive motion is approximately 2 min of tunnel time per second of flight time. This data acquisition rate will be improved significantly with the installation of new computing facilities.

Table 1. Characteristics of the F-15 Aircraft Simulated in Captive Testing

Configuration	Weight, lb,	c_g , percent c	I_x , slug-ft ²	I_y , slug-ft ²	I_z , slug-ft ²	I_{xz} , slug-ft ²	\bar{c} , ft	b, ft
NASA 3/8-Scale RPV	2,465	26.0	275	1,902	2,228	12	5.98	16.0185
Twin Tail Fighter, Clean	35,500	26.0	28,600	155,500	178,400	-600	15.94	42.7060
Twin Tail Fighter, MK-82 Bombs	47,550	26.0	53,480	162,270	206,580	-165	15.94	42.70607
Twin Tail Fighter, 500-gal Tanks	45,400	26.0	55,573	162,350	211,140	-500	15.94	42.70607

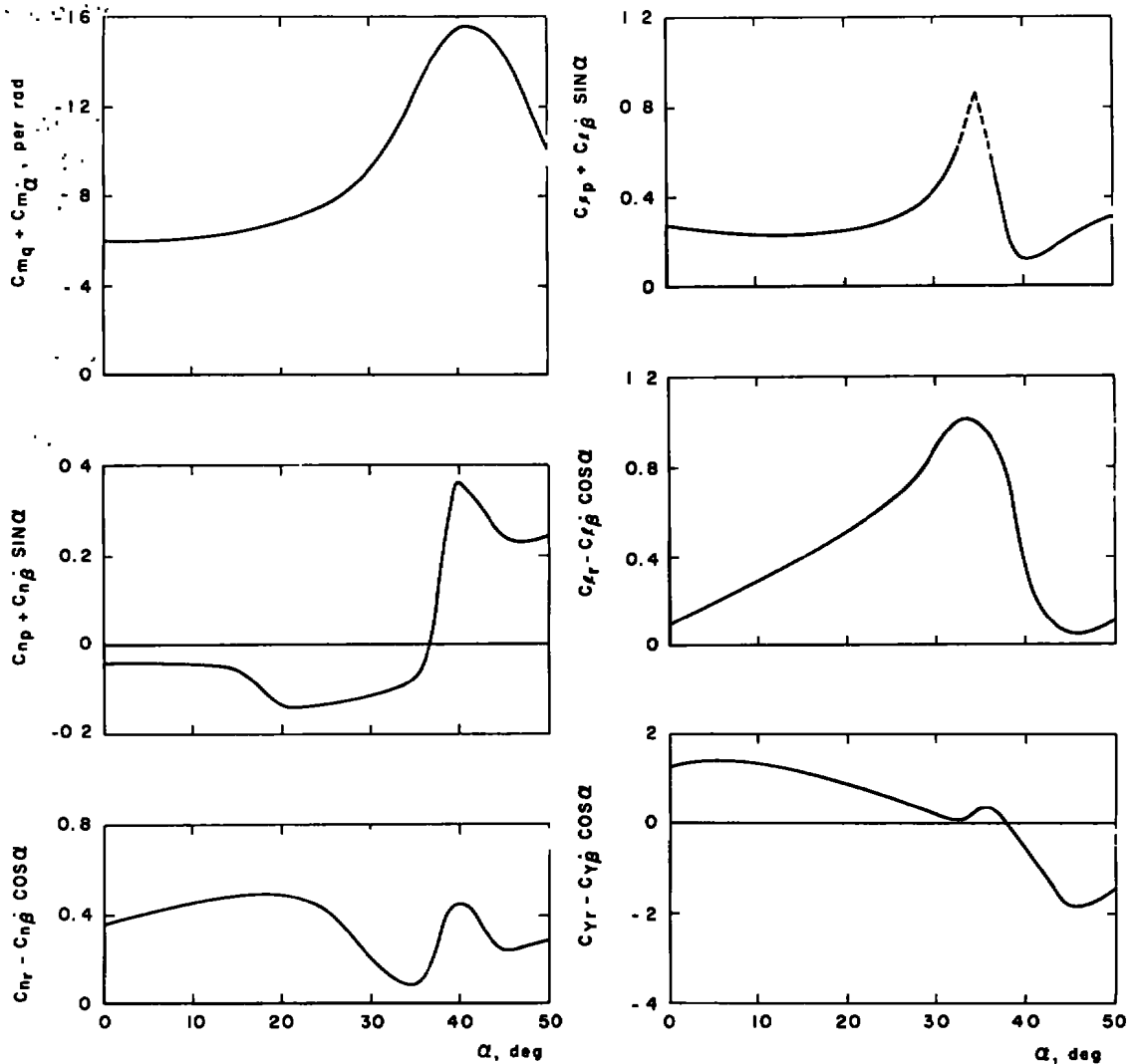


Figure 8. Dynamic stability derivatives representative of the NASA RPV model.

4.2 FLIGHT TEST-WIND TUNNEL DATA CORRELATION

Captive/flight data correlation for RPV longitudinal and lateral/directional motion are shown in Figs. 9 and 10, respectively. Each of these figures depicts three separate time history motions, one flight and two wind tunnel generated. The longitudinal maneuver (Fig. 9) was generated from a horizontal stabilizer (δ_h) doublet at a trimmed flight condition. The lateral/directional maneuver, Fig. 10, represents an aileron doublet obtained by differentially deflecting the model horizontal stabilizers (δ_D). The differential deflections occur about a nominal horizontal stabilizer setting (δ_h) of -15.8 deg. The flight

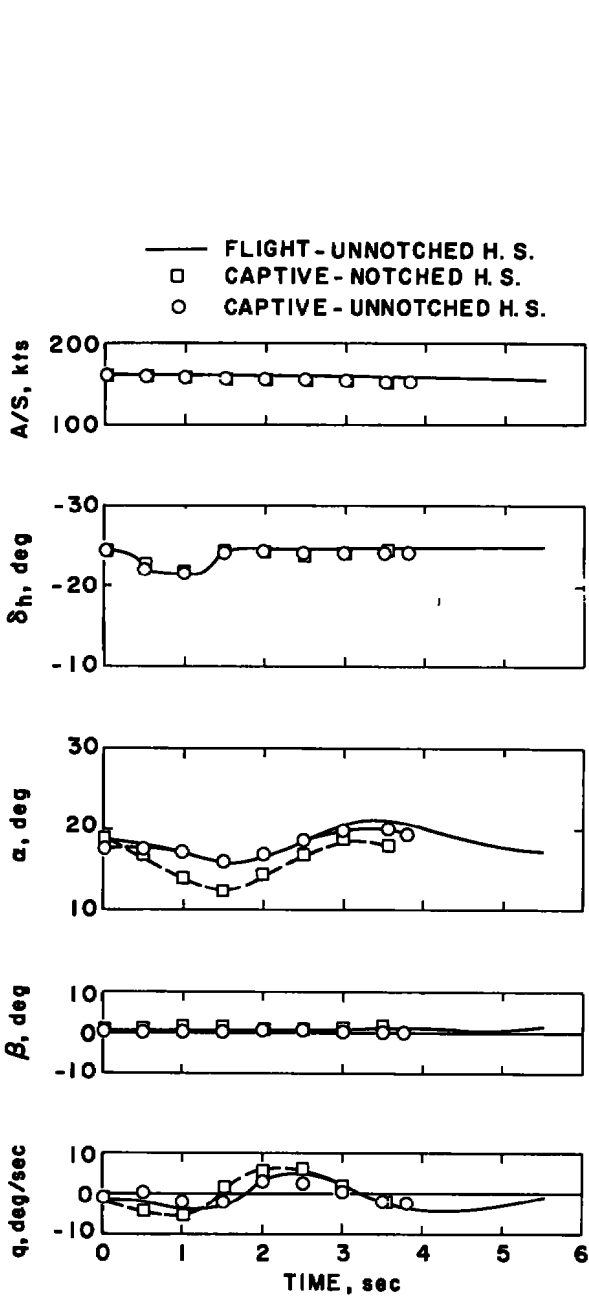


Figure 9. Flight/wind tunnel correlation of aircraft longitudinal motion.

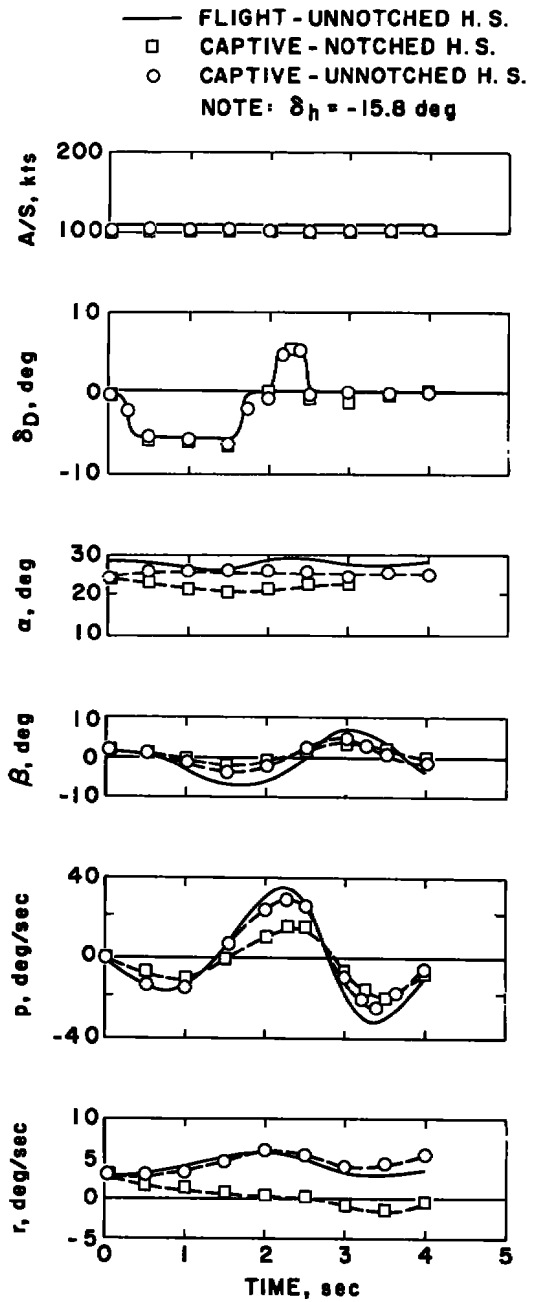


Figure 10. Flight/wind tunnel correlation of aircraft lateral motion.

data were acquired with an "unnotched" horizontal stabilizer configuration (Fig. 3). Flight test results, Ref. 7, with both "notched" and unnotched horizontal stabilizers showed no measurable change in aircraft trim angle of attack with either stabilizer. Because of this, the initial wind tunnel simulated motion was acquired with the 1/20-scale model utilizing an existing notched horizontal stabilizer. As seen in both the longitudinal and lateral/directional motion, the wind tunnel maneuvers with the notched stabilizer have motion frequencies near the flight data but show large deficiencies in amplitude. Also, the angle of attack at which the wind tunnel model trims for the lateral oscillations of Fig. 10 is approximately 4 to 6 deg lower than the RPV model for the nominal δ_h setting of -15.8 deg. Because of these differences the wind tunnel model was also tested with an unnotched horizontal stabilizer. Figure 11 presents angle-of-attack trim polars for the wind tunnel model with each horizontal stabilizer configuration and the RPV model with the unnotched stabilizer. Excellent agreement between the RPV and wind tunnel data with the unnotched horizontal stabilizers is evident at the lower angles of attack. Reasons for the discrepancies occurring at angles of attack above 22 deg are not known. The loss in tail effectiveness occurring at all angles with the wind tunnel model and the notched stabilizer may be attributed to the approximately 5.4 percent smaller planform area associated with the configuration. The reason this loss in planform area did not appreciably affect the RPV trim angle of attack reported in Ref. 7 was not investigated.

With the unnotched horizontal stabilizer incorporated on the wind tunnel model, new longitudinal and lateral/directional maneuvers were generated (Figs. 9 and 10, respectively). The amplitude discrepancies between RPV and captive motion decreased in all motion planes. The remaining small deficiencies in amplitude continue to be the result of the less effective horizontal stabilizer of the wind tunnel model at these high angles of attack as seen in Fig. 11.

An additional longitudinal motion correlation between flight and wind tunnel-generated data is presented in Fig. 12. In order that the unpowered flight vehicle could maintain airspeed with the da/dt rates shown in Fig. 12, the maneuver was initiated at a pitch and bank attitude of -40 and 72 deg, respectively, resulting in a wind-up turn type of maneuver. The maneuver required the RPV pilot to use aileron deflections which were not duplicated in the captive test. Fortunately, the aileron deflections were very small and the maneuver short ($t < 8$ sec); therefore, the aileron effect was minimized. However, if any but the most simple of aircraft maneuvers are to be simulated accurately in captive testing, programmable deflections of all three primary control surfaces, elevator, rudder, and aileron, must be available in the model.

Good agreement exists between the flight and captive longitudinal motion shown in Fig. 12. The small discrepancies between the angle of attack and pitch rate time histories

are related to the differences in the horizontal stabilizer effectiveness and the fact that the stabilizer deflection schedule (δ_h) was not simulated exactly in the wind tunnel model. Associated with the accelerated δ_h schedule is a corresponding da/dt rate which results in a variation in RPV airspeed. The changes which occurred were simulated by adjusting tunnel airspeed within approximately ± 5 kts of the flight value. Unrealistic deceleration rates not presented but experienced during checkout of the captive system verified that flight airspeed could be simulated under more severe "g" gradients without delay in data acquisition time.

The lateral oscillations experienced by the RPV and shown in the roll rate (p) time history of Fig. 12 were not seen in the captive generated motion. Although small aileron deflections were used for maintaining roll rate in the initial portion of the flight maneuver ($t < 2.5$ sec), the roll rate oscillations at higher angles of attack did not result from control deflections. The oscillations appear to have been excited by wing buffet experienced at high angles of attack, as noted in Ref. 7. Only steady-state forces and moments are measured in captive testing; therefore, any aircraft motion originating from unsteady aerodynamic loads cannot be simulated.

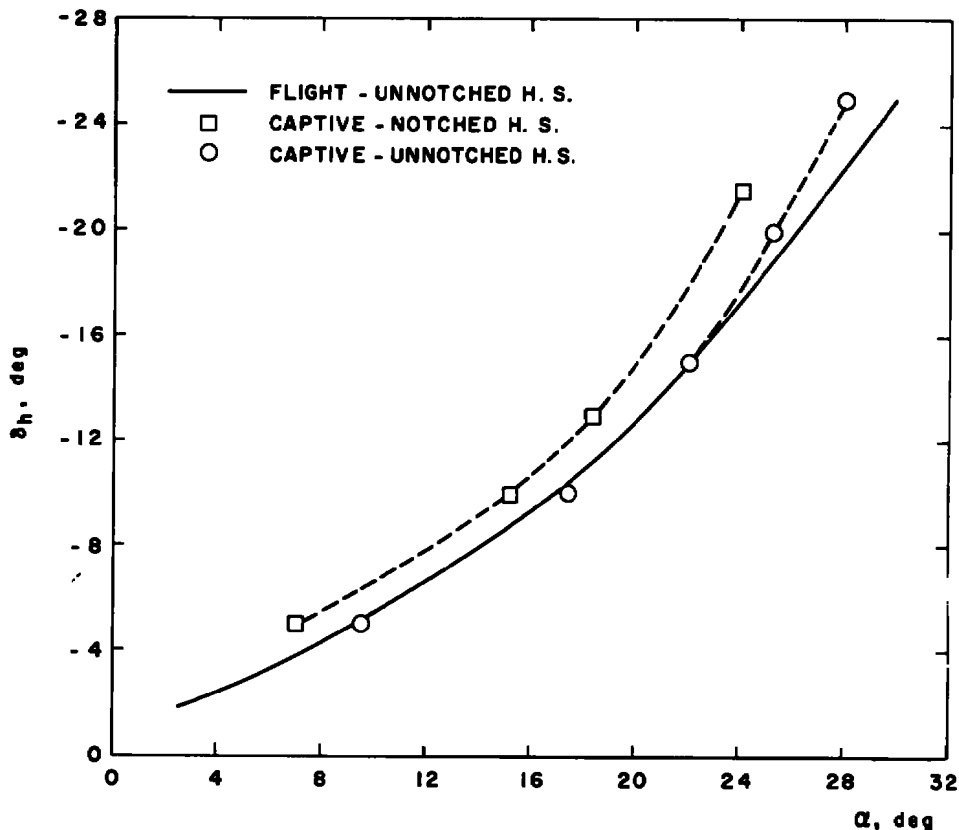


Figure 11. Model trim angle of attack.

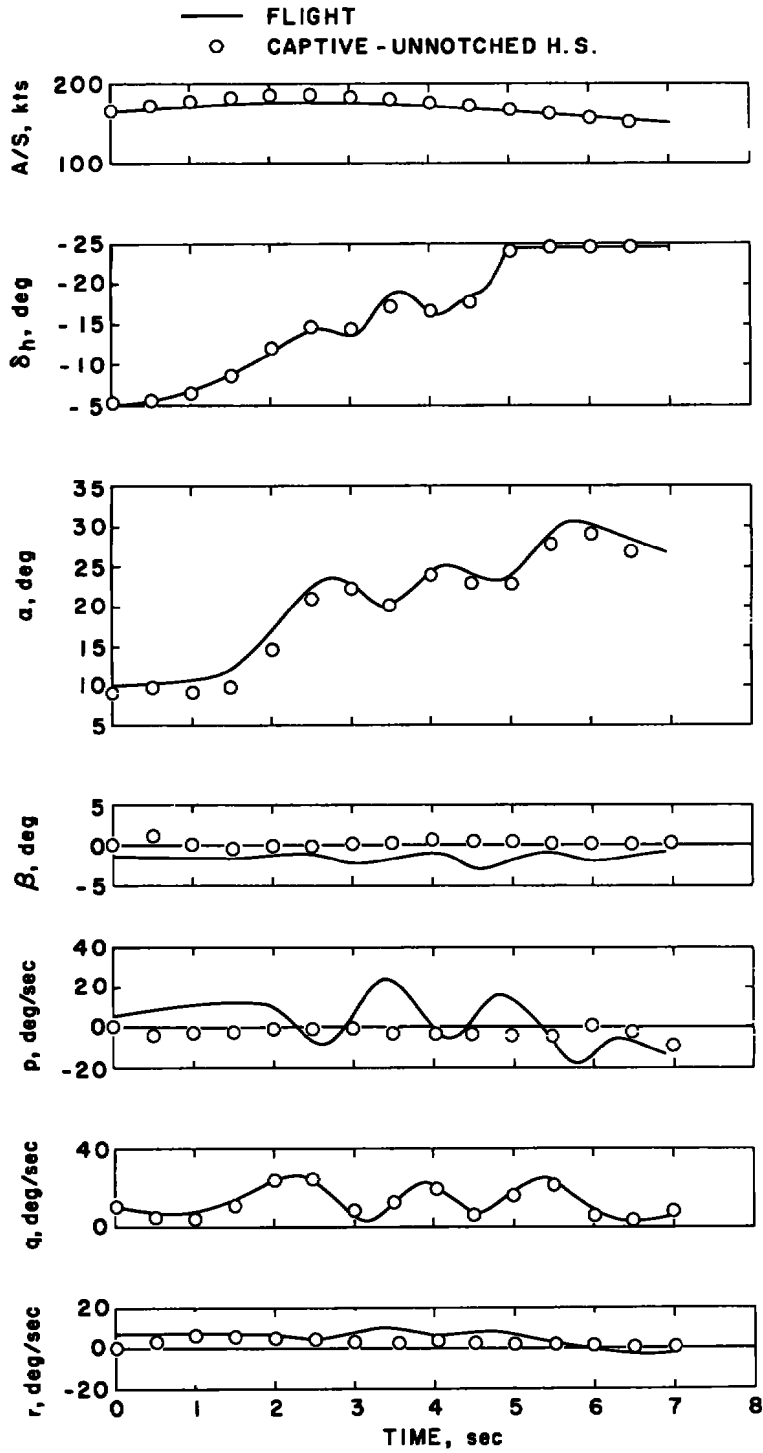


Figure 12. Flight/wind tunnel correlation of the aircraft wind-up turn maneuver.

To ascertain if the flight roll rate oscillation shown in Fig. 12 would have been achieved in the wind tunnel with the proper aerodynamic excitation, the captive motion shown in Fig. 13 was generated as follows. The wind tunnel model was initially trimmed longitudinally at 24 deg angle of attack and untrimmed directionally at 7 deg angle of sideslip. Because the maneuver was initiated in the untrimmed condition, a roll rate

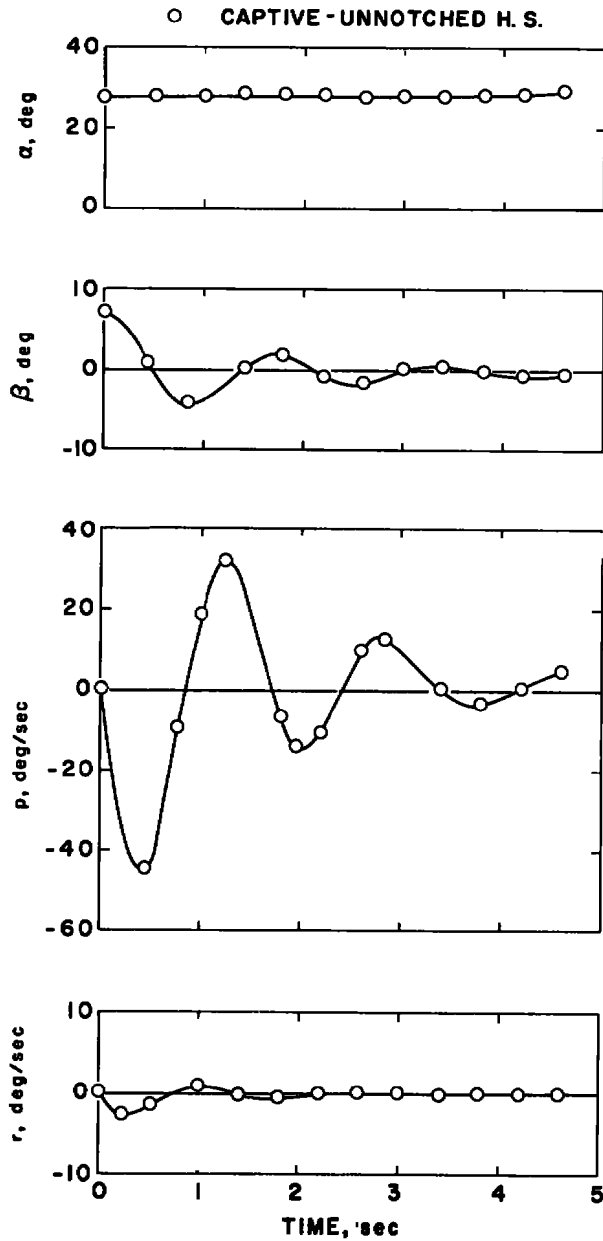


Figure 13. Simulated RPV lateral/directional motion.

oscillation was induced by the model effective dihedral ($-C_{l\beta}$). The period of the roll rate oscillation (Fig. 13) compares well to that experienced during the flight of the RPV (Fig. 12). Both motions possessed periods of approximately 1.5 sec, indicating that a good possibility of correctly simulating the RPV lateral motion exists if the unsteady aerodynamics could be modeled. Thus, when conducting captive testing for aircraft with severe buffet problems, some means of simulating the unsteady aerodynamics should be incorporated into the captive program.

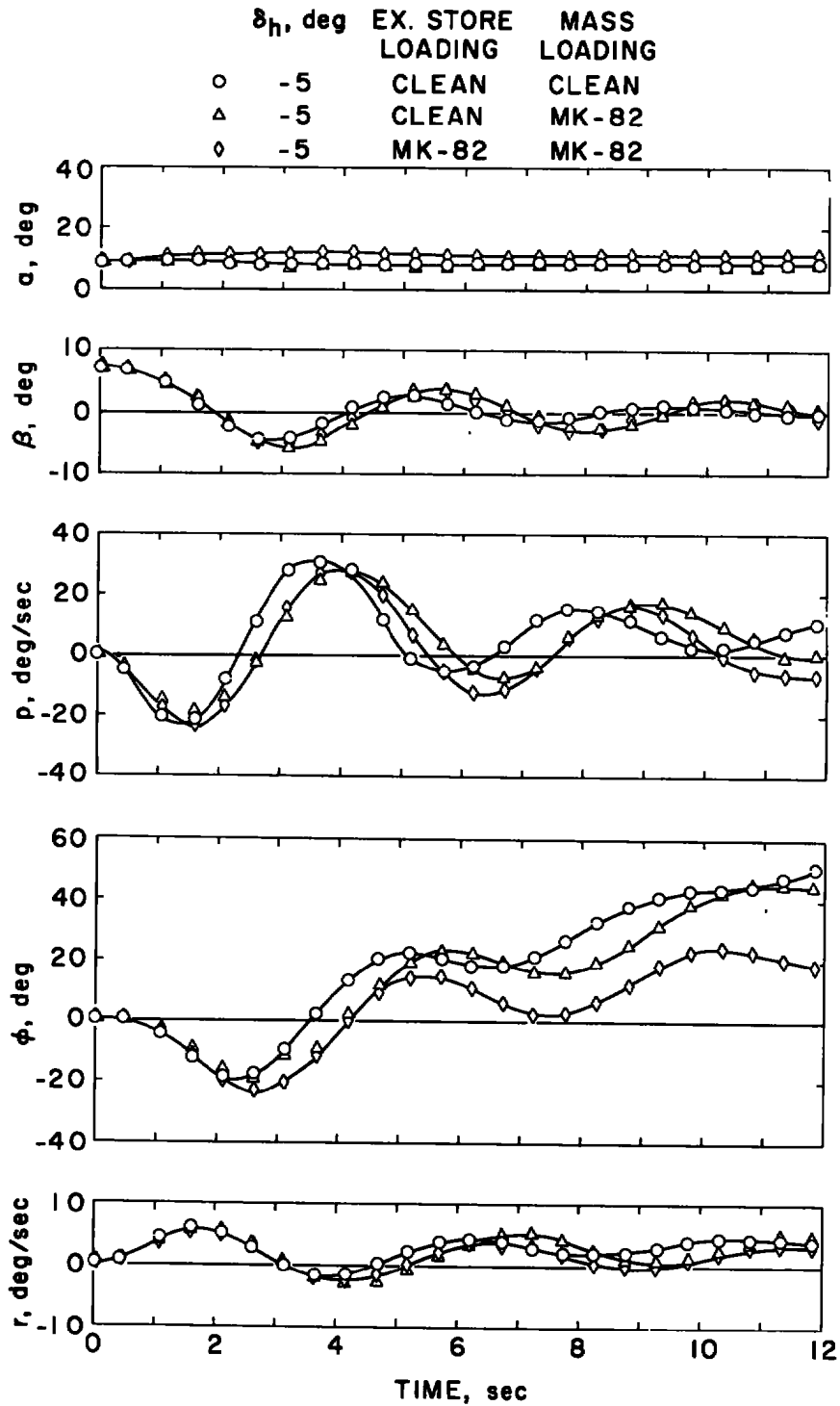
4.3 CAPTIVE TESTING EVALUATION

Aircraft flight characteristics may change drastically with the addition of external stores. Captive testing provides an accurate and efficient means of defining the changes without the generation of new aerodynamic data matrices and associated empirical prediction techniques. Examples of how aircraft flight characteristics may change with the addition of external stores and how these changes are defined with captive testing follow.

Ideally, to demonstrate how external stores may affect aircraft flight characteristics, a specific program of flight maneuvers (both longitudinal and lateral/directional) should be generated with the aircraft in both the clean and external store configurations. Since the 1/20-scale F-15 model utilized did not possess the control functions necessary for conducting such a program, a more basic lateral/directional stability maneuver was used. The maneuver is identical to that described in the previous section, with the model initially positioned in a longitudinal trim and directional out-of-trim orientation. Analysis of the resulting dutch roll motion provides indications of how the aircraft lateral/directional flight characteristics may be influenced by the addition of specific external stores.

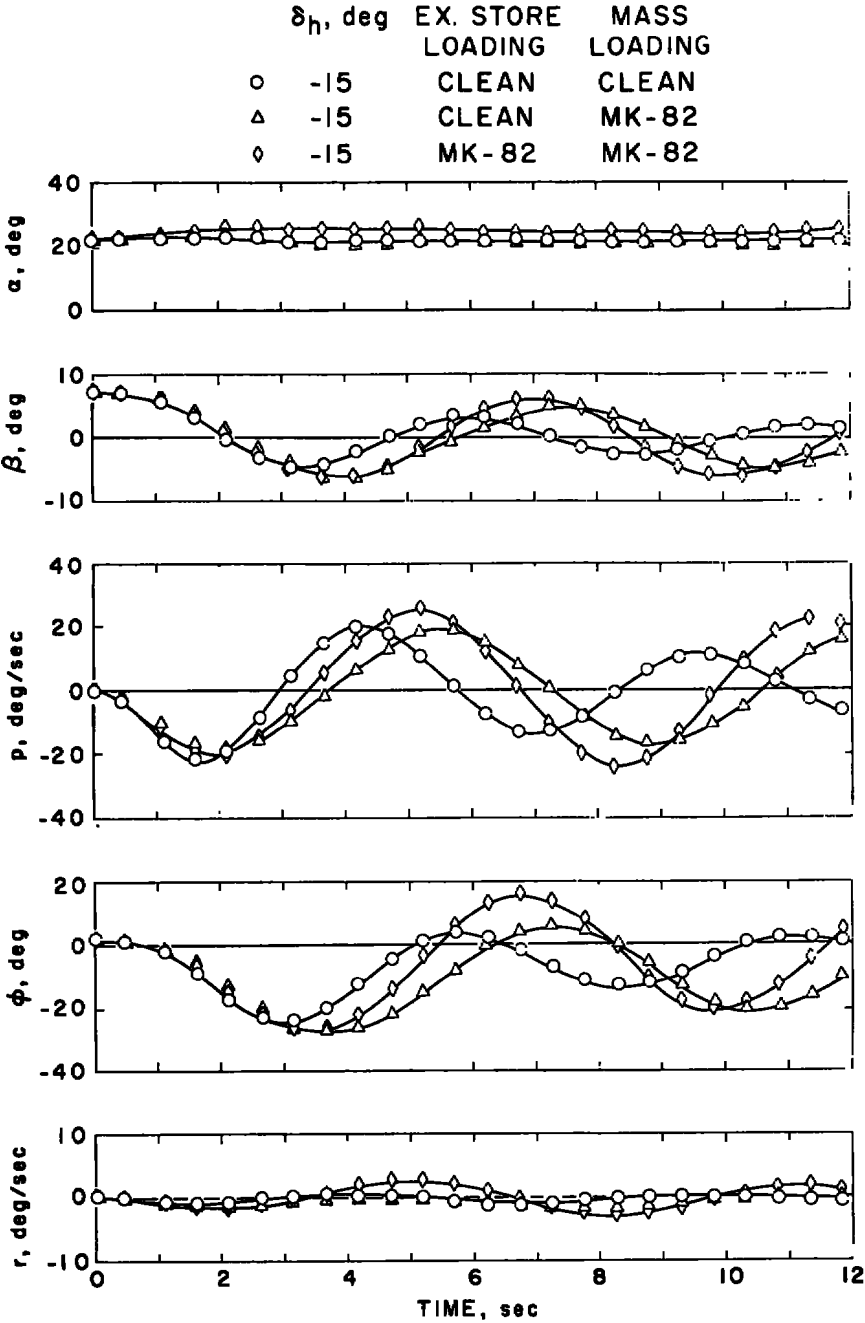
The mass characteristics simulated in the motion analysis are representative of the full-scale F-15 aircraft and are given in Table 1. Aircraft mass properties associated with the store configurations are approximate and should be considered only as representative of the actual values. The dynamic derivatives (used in the motion equations) were for the clean aircraft configuration as given in Fig. 8. The values of the dynamic derivatives were not changed for the different store configurations. Typical F-15 aircraft thrust characteristics as a function of Mach number, altitude, angle of attack, and angle of sideslip were included in the simulated maneuvers.

The time history motion of Fig. 14 shows how the F-15 lateral/directional flight characteristics may be affected by the change in the aircraft static aerodynamics associated with the addition of MK-82 external stores. The longitudinal trim angles of attack at which the motion is initiated correspond to horizontal stabilizer deflections of -5, -15, and -25 deg. The motion simulation occurred at a Mach number of 0.44 and a simulated

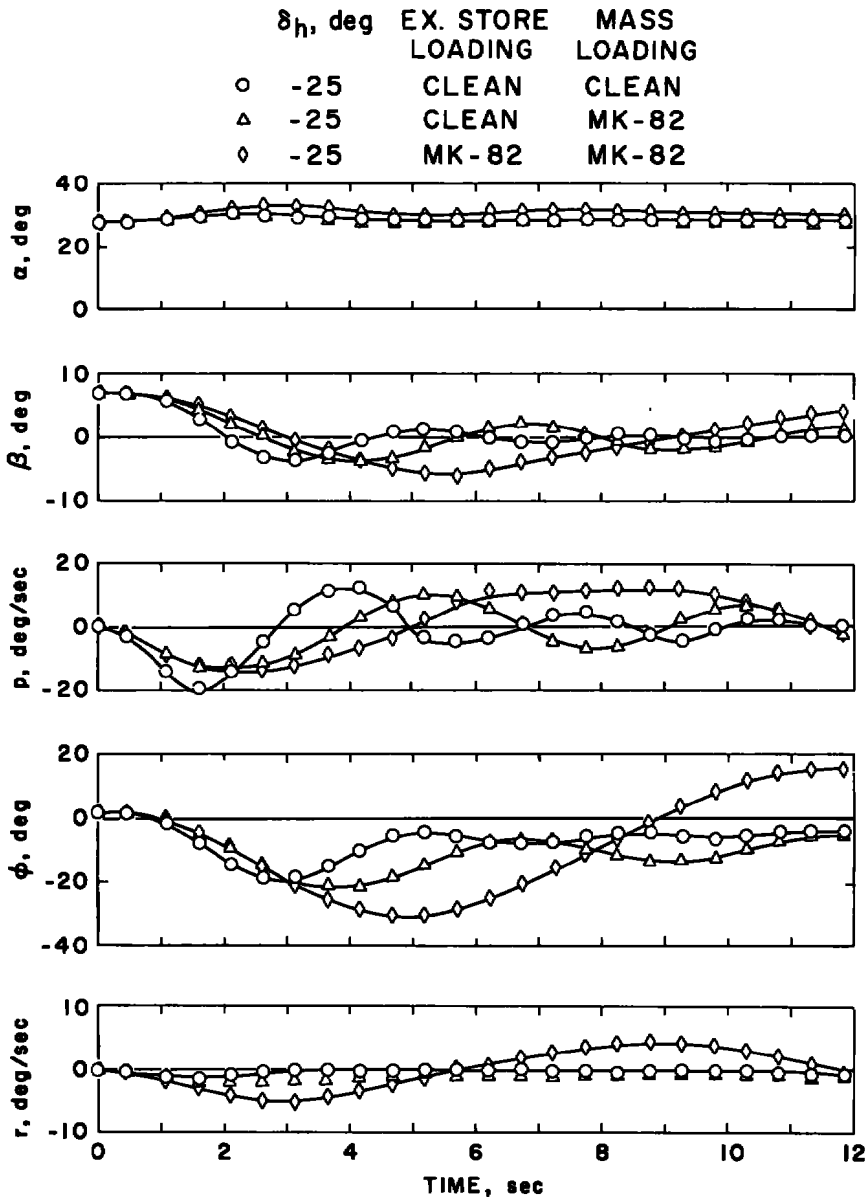


a. $\delta_h = -5$ deg

Figure 14. Lateral/directional motion of the F-15 model with MK-82 store configuration.



b. $\delta_h = -15$ deg
Figure 14. Continued.



c. $\delta_h = -25$ deg
Figure 14. Concluded.

altitude of 30,000 ft. Two sets of motion were generated using the clean aircraft configuration: one with mass characteristics of the clean aircraft, and one with the MK-82 configuration mass characteristics. Thus, the contribution that the additional MK-82 mass has on the lateral/directional stability characteristics is assessed. By also acquiring data with the MK-82 store configuration installed, changes resulting from the external stores influence on the aircraft static aerodynamics can be separated and assessed. A comparison

of the three sets of data in Fig. 14 shows that the static aerodynamic changes associated with the store loading have a significant effect on the aircraft motion period and damping. The period of the aircraft lateral motion along with the inverse time to damp to half amplitude ($1/T_{1/2}$) has been calculated and is presented in Fig. 15 as a function of angle of attack. The aircraft lateral stability is not significantly affected by the external store loading at the lower angles of attack, below 15 deg. A similar conclusion was obtained from the F-4 external store analysis presented in Ref. 1. However, at the higher angles of attack, above 15 deg, lateral stability is significantly changed as a result of the external stores' influence on the aircraft static aerodynamics. The damping parameter $1/T_{1/2}$ approaches a negative value, indicating oscillatory divergence, at an angle of attack near 30 deg. (The divergence is predicted to occur at approximately 34 deg when calculated with the $C_{n\beta}$ dynamic parameter discussed in Refs. 8 and 9). The data clearly show that the influence of external stores on the aircraft static aerodynamics at high angles of attack must not be neglected.

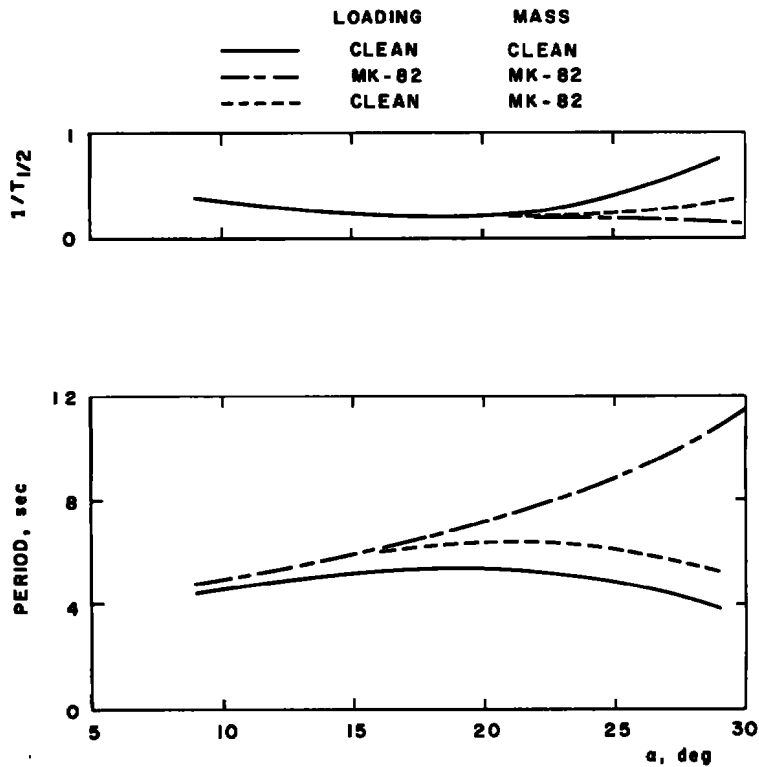
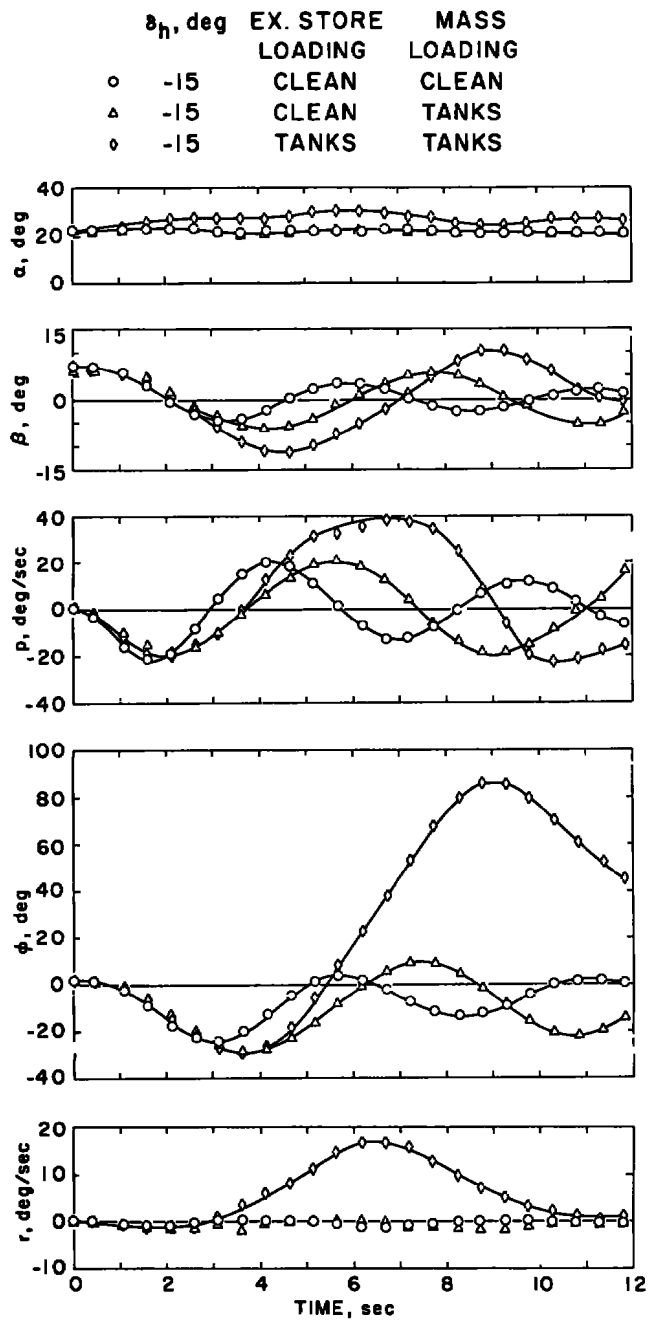


Figure 15. Damping and frequency of the F-15 model motion with MK-82 stores.

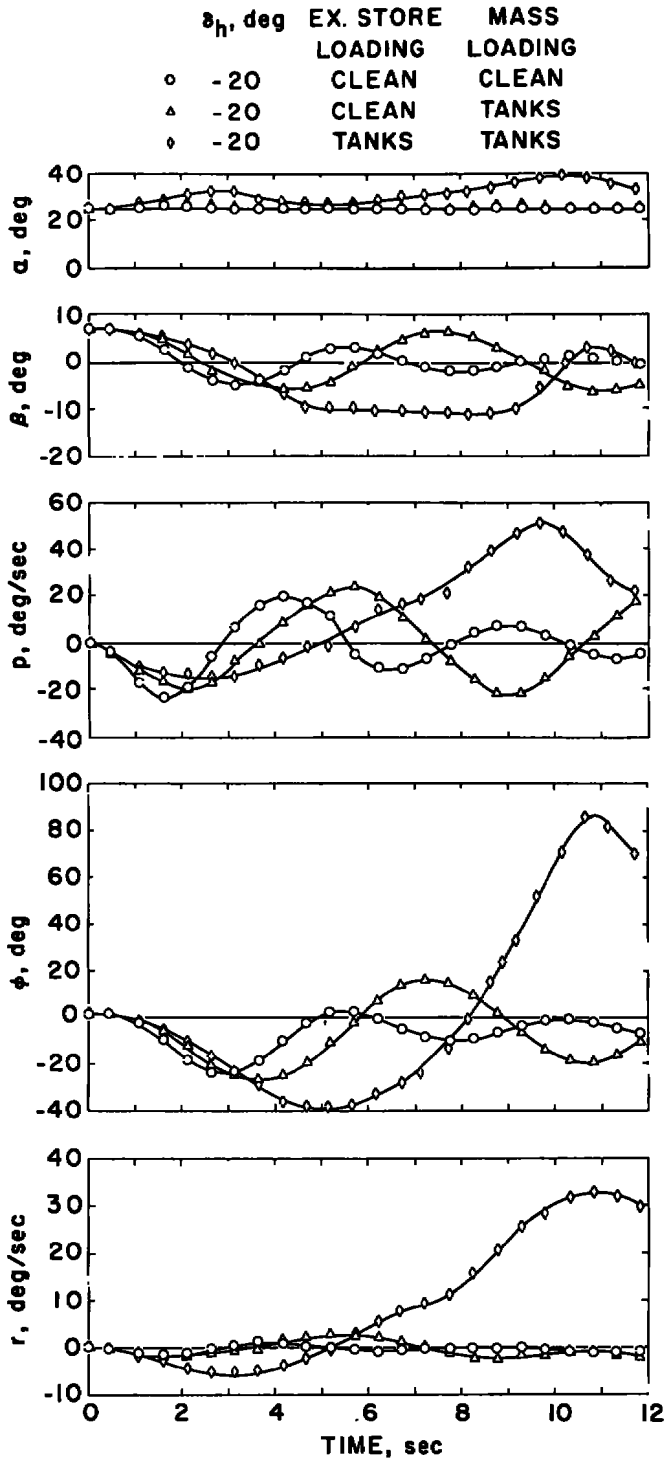
Additional lateral/directional stability data presented in Fig. 16 were generated with two 600-gal fuel tanks on the wing inboard pylon stations. The data were generated in a manner identical to those presented for the MK-82 configuration in Fig. 14. It should be noted that the time history motions, shown in Fig. 16, were obtained only at the higher angles of attack corresponding to horizontal stabilizer deflections of -15, -20, and -25 deg. Changing the clean F-15 mass characteristics to those of the 600-gal tank configuration without the corresponding aerodynamic changes resulted in a slight decrease in lateral stability and an increase in the motion period. These trends are identical to those shown in Fig. 14 for the change in mass characteristics from the clean aircraft configuration to the MK-82 configuration. Similarities in the two configurations are expected since the yaw/roll inertia ratios of both the tank and bomb configurations are of near equal magnitude (see Table 1). The lateral/directional motion of the 600-gal tank configuration (Fig. 16) shows the fuel tank aerodynamics to have a greater influence on the aircraft stability characteristics than did the MK-82 bomb configuration. The aircraft dutch roll motion is divergent with the 600-gal tanks at all angles of attack. The motion period increases with angle of attack until the dutch roll divergence observed at an angle of attack of approximately 20 deg (-15 deg stabilizer deflection) becomes a directional divergence at approximately 40 deg (-25 deg stabilizer deflection). The configuration also exhibits a longitudinal coupling in angle of attack not seen in the MK-82 bomb configuration. The coupling is aerodynamic since it was not observed in the clean configuration with the tanks mass properties. The time to damp to half amplitude and period were calculated and are presented in Fig. 17. It should be noted that the calculations of the lateral/directional motion presented are only approximations, since the angles of attack (Fig. 16) at which the parameters ($1/T_{1/2}$ and period) were calculated did not remain constant, and in most cases the motion was terminated before full oscillatory patterns developed.

Data presented in Figs. 16 and 17 again indicate the importance, when conducting an aircraft motion study, of accurately accounting for changes that occur in aircraft static aerodynamics caused by the addition of external stores. To successfully account for these changes empirically with the complex flow patterns associated with external store installations at high angles of attack is unlikely. To acquire new data matrices through conventional wind tunnel testing is unrealistic when several different configurations are involved. Captive testing provides the most efficient method of conducting aircraft motion studies for numerous different aircraft external configurations.



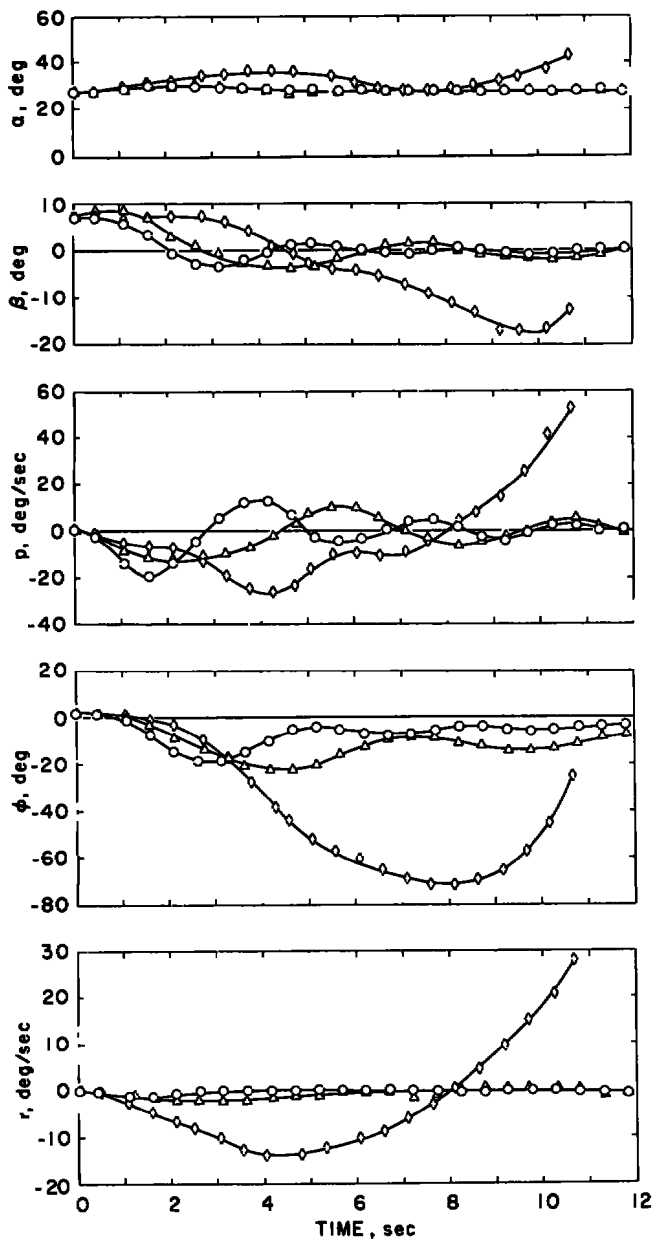
a. $\delta_h = -15$ deg

Figure 16. Lateral/directional motion of the F-15 model with 600-gal tanks.



b. $\delta_h = -20$ deg
 Figure 16. Continued.

δ_h , deg	EX. STORE	MASS
○	-25 CLEAN	CLEAN
△	-25 CLEAN	TANKS
◇	-25 TANKS	TANKS



c. $\delta_h = -25$ deg
 Figure 16. Concluded.

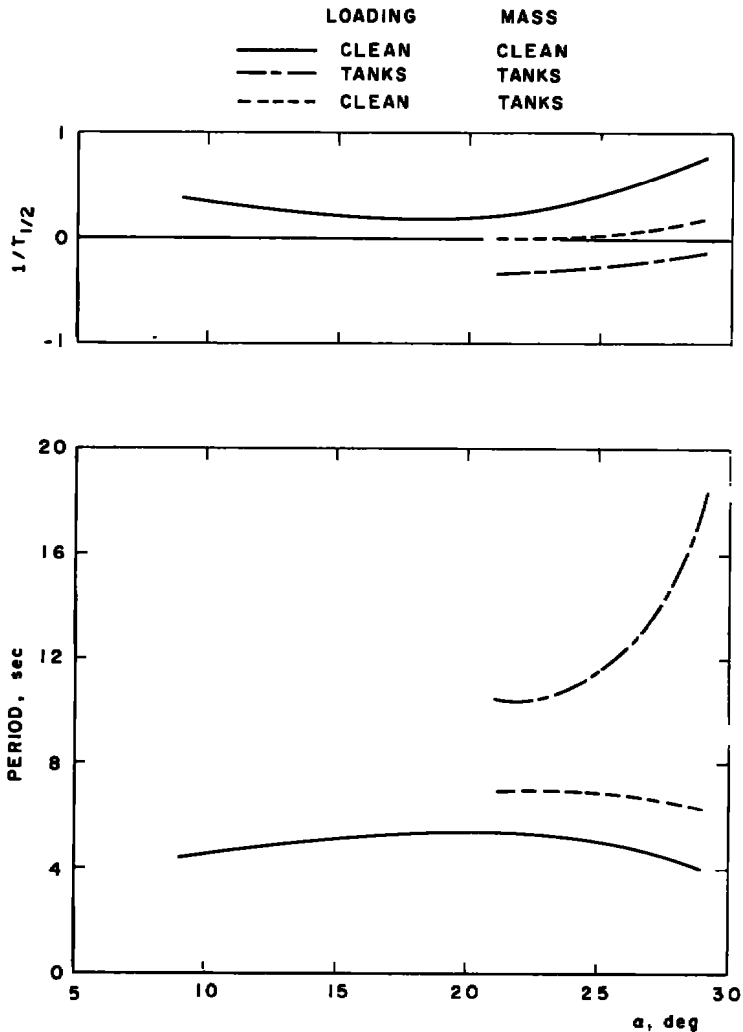


Figure 17. Damping and frequency of the F-15 model motion with 600-gal tanks.

5.0 CONCLUDING REMARKS

As a result of the analysis of the captive test program, the following conclusions and observations are noted:

1. The wind tunnel time required for simulating aircraft motion with the captive technique is approximately 2 min tunnel time per 1 sec of flight time. The data acquisition rate will be improved significantly with the installation of new computing facilities.

2. A comparison of captive-generated motion with NASA 3/8-scale F-15 flight motion shows good agreement in all planes of motion at angles of attack up to the onset of severe wing buffet.
3. When captive testing is conducted for aircraft with severe buffet problems, a means of simulating unsteady aerodynamics should be incorporated into the captive program.
4. Changes in aircraft static aerodynamic characteristics resulting from the addition of external stores must be accurately simulated to obtain correct high angle of attack motion information.
5. Captive testing should provide a direct simulation of Mach number and aerodynamic interference occurring with simultaneous control surface deflections although the latter were not utilized in the subject test because of wind tunnel model limitations.

REFERENCES

1. Weber, William B. "Effect of External Stores on the Stability, Control, and Drag Characteristics of the McDonnell Douglas F-4 Aircraft." Aircraft/Stores Compatibility Symposium Proceedings, Vol. III, Eglin AFB, 1969, pp 28-54.
2. Dyer, R. D. and Gallagher, R. D. "Technique for Predicting External Store Performance Effects on Aircraft Performance." Aircraft/Stores Compatibility Symposium Proceedings, Vol. I, Wright-Patterson AFB, 1971, pp 115-141.
3. Partridge, D. W. and Pecover, B. E. "An Application of the R.A.E. Wind-Tunnel/Flight Dynamics Simulator to the Low-Speed Dynamics of a Slender Delta Aircraft (HP 115)." R&M No. 3669, August 1969.
4. Butler, R. W. "Evaluation of a Wind Tunnel Technique to Determine Aircraft Departure Characteristics." AEDC-TR-73-183 (AD776317), March 1974.
5. Holleman, Euclid C. "Initial Results from Flight Testing a Large, Remotely Piloted Airplane Model." NASA TMX-56024, 1974.
6. Nichols, James H. "A Method for Computing Trajectories of Stores Launched from Aircraft." David Taylor Model Basin, DTMB-R-1878, November 1964.
7. Iliff, Kenneth. "F-15 Drone Flight Report - Flight D-9-15." NASA Flight Research Center, July 31, 1974.

8. Chambers, Joseph R. and Anglin, Ernie L. "Analysis of Lateral-Directional Stability Characteristics of a Twin-Jet Fighter Airplane at High Angles of Attack. NASA TND-5361, 1969.
9. Weissman, Robert. ."Criteria for Predicting Spin Susceptibility of Fighter-Type Aircraft. ASD-TR-72-48, 1972.

APPENDIX A EQUATIONS OF MOTION

The following equations were used in calculating the motion of the aircraft during captive testing.

$$\dot{p} = \frac{G_x}{I_x} + \frac{R_x}{I_x} + \frac{I_{xz}}{I_x} (\dot{r} + pq) + \frac{I_y - I_z}{I_x} qr$$

$$\dot{q} = \frac{G_y}{I_y} + \frac{R_y}{I_y} + \frac{I_{xz}}{I_y} (r^2 - p^2) + \frac{I_z - I_x}{I_y} rp$$

$$\dot{r} = \frac{G_z}{I_z} + \frac{R_z}{I_z} + \frac{I_{xz}}{I_z} (\dot{p} - qr) + \frac{I_x - I_y}{I_z} pq$$

$$\dot{u} = \frac{x}{m} + \frac{T_x}{m} + n_1 g - qw + rv$$

$$\dot{v} = \frac{y}{m} + n_2 g - ru + pw$$

$$\dot{w} = \frac{z}{m} + \frac{T_z}{m} + n_3 g + qv - pv$$

The aerodynamic forces and moments used in the simulation were as follows:

$$x = x(a, \beta)$$

$$y = y(a, \beta) + \rho \frac{v_\infty S b}{4} (C_{Y_r} r + C_{Y_\beta} \dot{\beta})$$

$$z = z(a, \beta)$$

$$G_x = G_x(a, \beta) + \rho \frac{v_\infty S b^2}{4} C_{\ell_p} p + C_{\ell_r} r + C_{\ell_\beta} \dot{\beta}$$

$$G_y = G_y(a, \beta) + \rho \frac{v_\infty S \bar{c}^2}{4} (C_{m_q} q + C_{m_\alpha} \dot{\alpha})$$

$$G_z = G_z(a, \beta) + \rho \frac{v_\infty S b^2}{4} (C_{n_r} r + C_{n_p} p + C_{n_\beta} \dot{\beta})$$

where $x(a, \beta)$, $y(a, \beta)$, $z(a, \beta)$, $G_x(a, \beta)$, $G_y(a, \beta)$, and $G_z(a, \beta)$ are the aerodynamic static forces and moments generated in the wind tunnel.

NOMENCLATURE

A/C	Aircraft
A/S	Air speed, kts
b	Wing span, ft
C_{ℓ}	Rolling-moment coefficient, $M_x/q_{\infty}Sb$
$C_{\ell_{\beta}}$	Static derivative or rolling moment due to sideslip, $\partial C_{\ell}/\partial \beta$
$C_{\ell_{\dot{\beta}}}$	Lateral acceleration derivative in roll, $\partial C_{\ell}/(\partial \dot{\beta}b/2V_{\infty})$
C_{ℓ_p}	Dynamic damping derivative in roll, $\partial C_{\ell}/(\partial pb/2V_{\infty})$
C_{ℓ_r}	Dynamic cross-derivative or rolling moment due to yawing, $\partial C_{\ell}/(\partial rb/2V_{\infty})$
C_m	Pitching-moment coefficient, $M_y/q_{\infty}S\bar{c}$
C_{m_q}	Dynamic damping derivative in pitch, $\partial C_m/(q\bar{c}/2V_{\infty})$
$C_{m_{\dot{\alpha}}}$	Longitudinal acceleration derivative in pitch, $\partial C_m/(\partial \dot{\alpha}\bar{c}/2V_{\infty})$
C_n	Yawing-moment coefficient, $M_z/q_{\infty}Sb$
$C_{n_{\beta}}$	Static derivative of yawing moment due to sideslip, $\partial C_n/\partial \beta$
$C_{n_{\dot{\beta}}}$	Lateral acceleration derivative in yaw, $\partial C_n/(\partial \dot{\beta}b/2V_{\infty})$
C_{n_p}	Dynamic cross-derivative of yawing moment due to rolling, $\partial C_n/(\partial pb/2V_{\infty})$
C_{n_r}	Dynamic damping derivative in yaw, $\partial C_n/(\partial rb/2V_{\infty})$
$C_{n_{\beta}}$, dyn	Directional divergence parameter, $C_{n_{\beta}} - (I_z/I_x) C_{\ell_{\beta}} \sin \alpha$
C_Y	Side force coefficient, $F_Y/q_{\infty}S$
$C_{Y_{\dot{\beta}}}$	Lateral acceleration derivative in side force, $\partial C_Y/(\partial \dot{\beta}b/2V_{\infty})$
C_{Y_r}	Dynamic derivative of side force due to yawing, $\partial C_Y/(\partial rb/2V_{\infty})$
\bar{c}	Mean geometric chord, ft

cg	Aircraft center of gravity
F_Y	Side force, lb
G_x, G_y, G_z	Components of the aerodynamic moments about the X_B , Y_B , and Z_B axes, respectively, ft-lb
H.S.	Horizontal stabilizer
I_x, I_y, I_z	Moments of inertia about X_B , Y_B , and Z_B axes, respectively, slug-ft ²
I_{xz}	Product of inertia, slug-ft ²
M_x	Rolling moment, ft-lb
M_y	Pitching moment, ft-lb
M_z	Yawing moment, ft-lb
n_1, n_2, n_3	Direction cosines of body axis relative to earth axis
p, q, r	Aircraft roll, pitch, and yaw rates about the X_B , Y_B , and Z_B axes, respectively, deg/sec
q_∞	Dynamic pressure, lb/ft ²
R_x, R_y, R_z	Moment contributions from engine thrust about the X_B , Y_B , and Z_B axes, respectively, ft-lb
S	Wing area, ft ²
T_x, T_z	Components of engine thrust along the X_B and Z_B axes, respectively, ft/sec
$T_{1/2}$	Time required for the amplitude of oscillation to decrease by a factor of 2, sec
t	Simulated flight time, sec
u,v,w	Linear velocity components along the X_B , Y_B , and Z_B axes, respectively, ft/sec
V_∞	Free-stream velocity, $(u^2 + v^2 + w^2)^{1/2}$, ft/sec

X_B, Y_B, Z_B	Right-hand body axis cartesian coordinates, X positive forward
x, y, z	Components of the aerodynamic forces along the X_B , Y_B , and Z_B axes, respectively, lb
α	Angle of attack, $\tan^{-1} w/u$, deg or rad
β	Angle of sideslip, $\sin^{-1} v/V_\infty$, deg or rad
δ_D	Differential stabilizer deflection, deg
δ_h	Horizontal stabilizer positions, deg, positive trailing edge down
ρ	Simulated air density, slugs/ft ²
ϕ	A/C bank angle, deg

NOTE: Dot over symbol indicates derivative with respect to time.